university of groningen

faculty of science and engineering

The relation between the ED-3 halo substructure and the globular cluster NGC 3201

Dominic-Andreas Popp

university of groningen / faculty of science and engineering

University of Groningen

Bachelor Thesis

To fulfill the requirements for the degree of
Bachelor of Astronomy
at University of Groningen under the supervision of
A. Helmi and H. C. Woudenberg

Dominic-Andreas Popp (s4140427)

February 12, 2025

Contents

Page

Abstract **4**

1 Introduction **5**
1.1 Anatomy of the Milky Way 5
1.2 Accretion 5
1.3 NGC 3201 and ED-3 6
1.4 A possible association between ED-3 and NGC 3201 8

2 Methodology **11**
2.1 Short description 11
2.2 Initial properties: ED-3 progenitor 11
2.3 AGAMA 12
2.4 Backwards orbit integration 13
2.5 Angular Momentum and Energy 14

3 Analysis **15**
3.1 NGC 3201 centering 15
3.2 ED-3 Centering with $r_{1/2} = 0.25$ kpc 17
3.3 ED-3 centering with $r_{1/2} = 0.02$ kpc 22
3.4 Distribution in IoM 23
3.5 Is there a link between ED-3 and NGC 3201? 24

4 Conclusion **26**

Acknowledgements **27**

Abstract

The Milky Way's stellar halo is thought to be partly made up of the debris of past merger events. In merging with the Milky Way, these systems can also bring in their own globular clusters (GC). NGC 3201 is a GC on a retrograde orbit in the Galactic halo, which likely has an accreted origin. Dodd et al. [2024] propose a possible connection between NGC 3201 and the accreted substructure ED-3, that was identified in the solar neighborhood (Dodd et al. [2023]), based on their similar orbits and proximity in integrals of motion space. To further research the connection between the two, we performed test-particle simulations, using AGAMA, of a dwarf galaxy-like system orbiting in a Milky Way potential with a range of characteristics that could represent ED-3. Particularly, we consider three different masses (5 x 10^5, 10^6, 5 x 10^6 $M_\odot$) and 2 different sizes ($r = 0.25$, $r = 0.02$ kpc, corresponding to a dwarf galaxy and massive GC progenitor, respectively) for the ED-3 progenitor, which we study for three integration timespans (5 Gyr, 7.5 Gyr and 10 Gyr) and different progenitor centerings. We compare the overlap in velocity space, the overlap in integrals of motion space, and the ratio of $N(v_z > 0)/N(v_z < 0)$ between the simulated particles that are in a local volume at the present day and the ED-3 data.

Our analysis suggests that NGC 3201 cannot be the core of ED-3, as recentering the progenitor to NGC 3201's past orbit does not provide a good match with the observed ED-3 data. Instead, when recentering to an ED-3 star, we find that a dwarf-like system ($r = 0.25$ kpc) with a mass of 5 x 10^6 $M_\odot$ and integration time of 10 Gyr provides a good match, as also the $N(v_z > 0_{sim})/N(v_z < 0)_{sim}$ ratios are similar. Similar results are found for a massive globular cluster-like system ($r = 0.02$ kpc) with mass of 5 x 10^6 $M_\odot$ and integration time of 7.5 Gyr. In both cases, simulated particles are found in the proximity of NGC 3201 in position and velocity space. These findings suggest a connection between ED-3 and NGC 3201 by having the same tidally disrupted progenitor.

1 Introduction

1.1 Anatomy of the Milky Way

The Milky Way galaxy, of which a schematic representation is shown in Figure 1 is a barred spiral galaxy with a central bulge, a thin and thick stellar disk, and a diffuse stellar halo [Bland-Hawthorn and Gerhard, 2016]. The Milky Way houses an approximate 10^{11}, stars, while it's mass is roughly $10^{12} M_{\odot}$ [Watkins et al., 2019].

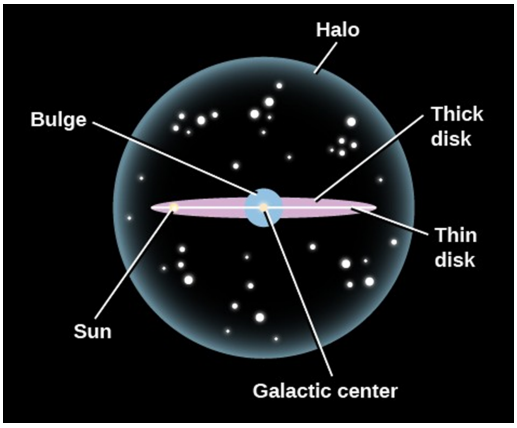

Figure 1: Simplified diagram showing the main components of the Milky Way, namely the bulge (circle in the center), halo (large circle with blue outline), and think and thick stellar disks. Also the position of the Galactic Center and Sun are indicated. Reproduced from CalPoly [2025].

The thin disk, 350 pc mean scale height [Carroll and Ostlie, 2007] and 3.5 kpc scale length [Sparke and Gallagher, 2007] hosts the galaxy's spiral arms, which are regions of higher density. These arms are sites of active star formation, populated by young, bright stars, star clusters, and regions of gas and dust known as molecular clouds. The Sun is located within the thin disk, approximately 8.2 kpc from the Galactic Center [McMillan, 2017]. It resides in a Local Arm [Vallée, 2018], situated close to the Orion Arm, between two of the Milky Way's larger spiral arms, the Sagittarius Arm and the Perseus Arm.

The thick disk is more extended vertically and contains older stars with lower metallicity, while also less densely populated than the thin disk [Bensby and Feltzing, 2009]. Enclosing the entire galaxy is the stellar and dark matter halo, a roughly spherical region that contains ancient stars, globular clusters, dwarfs, and dark matter [Forbes and Bridges, 2010]. The Milky Way's dark matter halo extends far beyond the visible components of the Milky Way [Battaglia et al., 2005]. The halo also hosts stellar streams—remnants of smaller galaxies and globular clusters that have been tidally disrupted by the Milky Way [Price-Whelan et al., 2019].

1.2 Accretion

Accretion is a fundamental process in formation of galaxies, where larger galaxies grow by gravitationally capturing and assimilating smaller galaxies, along with their stars, gas, and dark matter. This phenomenon is crucial to the Milky Way's evolution, as shown by its interactions with numerous dwarf galaxies and the presence of globular cluster populations. These systems, with stellar masses ranging from $10^4 M_{\odot}$ to $10^9 M_{\odot}$ (from GCs [Bragaglia et al., 2017] to DGs [Liu et al., 2015]). One example is the Sagittarius Dwarf Spheroidal from Figure 2 that shows signs of past interactions. From accretion events like this, stellar streams are formed, such as the Sagittarius Stream, that are relics of disrupted dwarf galaxies [Martínez-Delgado et al., 2001].

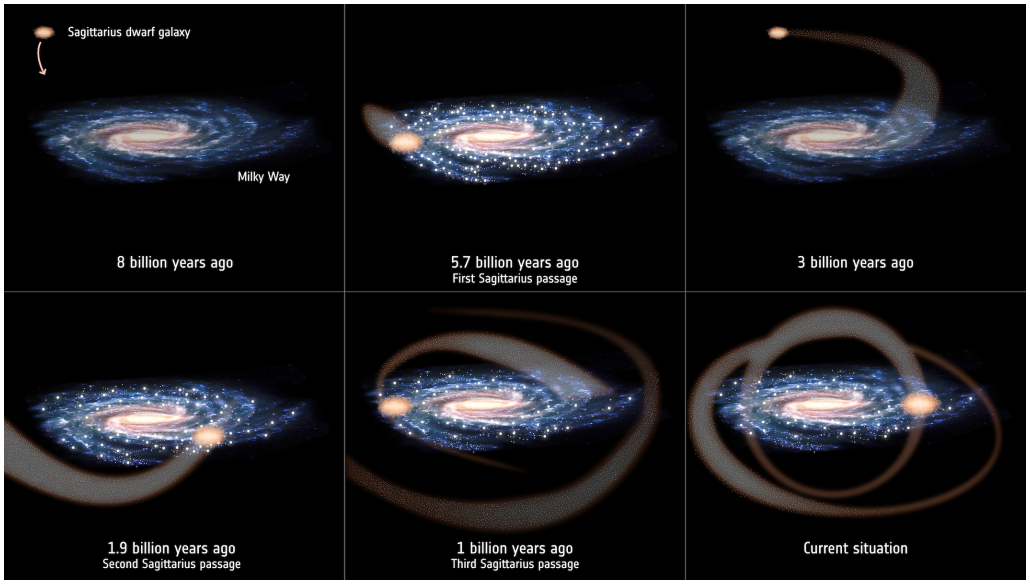

Figure 2: Accretion and disruption of the Sagittarius dwarf galaxy into the Milky Way, illustrating how the Sagittarius Stream formed over time. Reproduced from European Space Agency (ESA) [2020].

Globular clusters, dense groups of ancient stars, that bear the mark of accretion. Some were formed within the Milky Way, while others were accreted from captured galaxies, as suggested by their distinct metallicities and kinematics. Globular clusters are among the oldest known stellar populations in the Galaxy, their ages often exceeding 10^{10} years, and are thought to have formed during the early stages of the Milky Way's life [Jimenez, 1998]. There are approximately 150–160 known globular clusters in the Milky Way [Harris, 2010].

For example, the Sagittarius Dwarf Spheroidal Galaxy, which is currently being tidally disrupted, has already lost stellar mass to form the Sagittarius Stream — a vast structure that wraps around the Milky Way multiple times [Majewski et al., 2003]. As can be seen in Figure 2, multiple passes have been made around the MW since it's accretion process started.

Together, globular clusters, dwarf galaxies, and tidal remnants paint a vivid picture of the Milky Way's hierarchical growth, driven by the accretion and merging of smaller systems. By studying these objects and structures, we can trace the galaxy's evolution from its earliest times to its current state. The combination of observational data, such as that provided by Gaia, and other large-scale surveys, combined with simulations of galaxy formation, allows for a more complete understanding of processes that shaped the Milky Way, revealing not only its structure, but also its connections to the broader universe.

1.3 NGC 3201 and ED-3

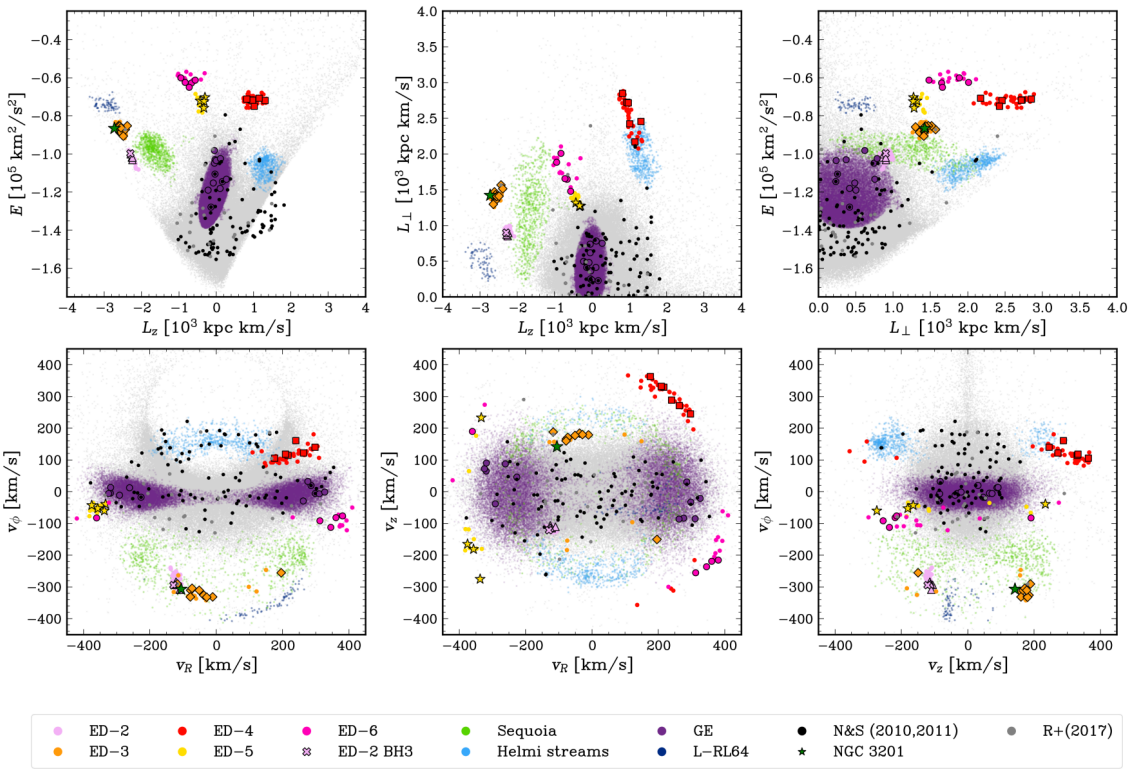

Figure 3: IoM (top row) and velocity (bottom row) space of local halo stars, in light grey. A number of halo substructures are shown by colored markers, with ED-3 being shown in orange. Stars for which chemical abundances have been derived are shown with outlined darker symbols. The position of NGC 3201 is shown as a green star, showing the proximity to ED-3 in IoM space. Reproduced from Dodd et al. [2024]

More than 50 % of GC's in the MW are of extra-galactic origin, with 35 % of those being associated to known merger events, as suggested by Massari et al. [2019]. One of these presumably merger acquired GC's is NGC 3201, which is a prominent globular cluster spanning 8.26 pc half-mass radius [Baumgardt, Accessed 2025]. NGC 3201 is classified as a relatively low-concentration globular cluster with a distinctive low central stellar density compared to other globular clusters [Webb et al., 2005]. Because of its retrograde motion, it has been suggested that NGC 3201 could have an extragalactic origin and may have been accreted into the Milky Way from a nearby dwarf galaxy Sariya et al. [2017].

Figure 4: NGC 3201 as a color composite image. Observed using the WFI instrument on the ESO/MPG 2.2-m telescope at La Silla. Reproduced from Observatory [2021]

Research indicates that NGC 3201 is inhomogeneous, with different stellar populations

found at varying distances from its center. This feature is rare among globular clusters, and NGC 3201, along with Messier 4, is one of only a few clusters that display such inhomogeneity. The stars in the outer regions tend to be hotter and more massive than those near the center, which have a cooler, redder hue [Kravtsov et al., 2010].

The ED-3 substructure is one of six groups of ED stars found as possible merger candidates. It is composed of 16 member stars with a bimodal distribution in z-velocity space. Located in the solar neighborhood, it shares similarities with the globular cluster NGC 3201 in several ways, particularly in their orbital dynamics and Integrals of Motion (IoM) characteristics. It was discovered due to the clump-like formation shown in Figure 3 in the Dodd et al. [2023] study. Particularly, it was shown in Dodd et al. [2024] that ED-3 (orange in Figure 3) lies very close and tight with NGC 3201 in the space of IoM parameters, shown with the green star, which suggests a possible connection between the two.

1.4 A possible association between ED-3 and NGC 3201

Figure 5 shows the orbit of NGC 3201 and ED-3 stars integrated backward and forward for 0.5 Gyr. While they do not show overlap directly, they are similar, suggesting an association. The green shading emphasizes sampled orbits of NGC 3201 and how the orbit of the globular cluster overlaps with ED-3 stars highlighted in blue and red after some revolutions. The $v_z > 0$ ED-3 star (shown in blue) shows overlap with the trailing arm of NGC 3201, although three radial revolution away from NGC 3201, whilst the $v_Z < 0$ star (shown in red) overlaps with the trailing arm. The Gjöll stream [Ibata et al., 2019, Hansen et al., 2020] has also been associated with NGC 3201 but it does not overlap with ED-3. The connection between ED-3 and NGC 3201, while kinematically linked, cannot be fully explained by originating as tidal stream debris of the globular cluster. This is also supported by the much broader metalicity distribution of ED-3, than that of NGC 3201, as is shown in (Figure 6 and Figure 7). This suggests that ED-3 originated from a disrupted dwarf galaxy.

Chemical comparisons of the stars in ED-3 and NGC 3201 were performed by Dodd et al. [2024] by examining light-element abundances, such as [Mg/Fe], [Na/Fe], and [Al/Fe], where ED-3 members were found to have lower values in all of these ratios. In comparison to NGC 3201, ED-3 has a similar [Mg/Fe] spread, while [Na/Fe] and [Al/Fe] show smaller dispersion. While ED-3 stars are, on average, bluer and exhibit a lower metallicity than NGC 3201 stars, there is some overlap in the populations, especially in stars with higher metallicities as seen in Figure 6. NGC 3201's light element spread suggests the presence of multiple stellar populations, the lack of such a spread for ED-3 suggests that ED-3 is not the tidal debris from the globular cluster.

The goal of this thesis is to investigate the following questions:

1. Is there any relationship between globular cluster NGC3201 and ED-3 substructure?
2. What are the conditions in which the observations and relation can be reproduced?

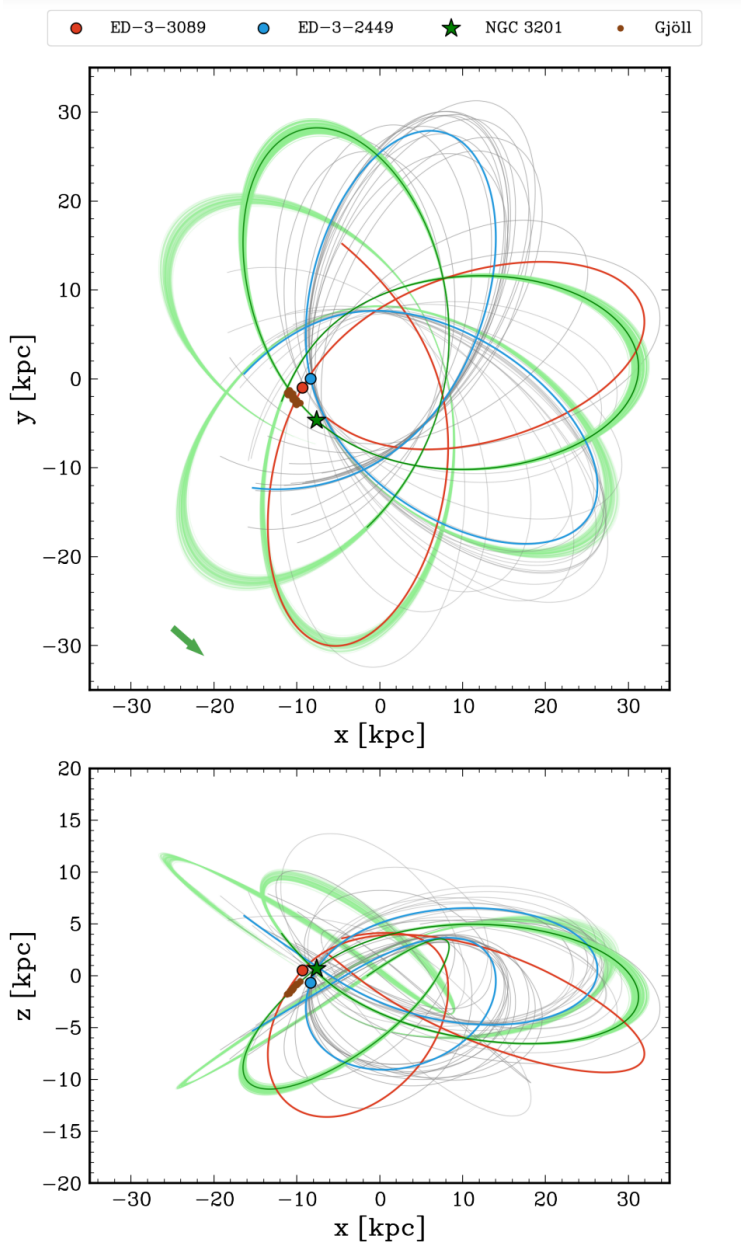

Figure 5: The orbits of ED-3 stars (shown in grey) and NGC 3201 (shown in green) were integrated backward and forward for 0.5 Gyr. The orbits of ED-3-3089 (red), having $v_z < 0$ and ED-3-2449 (blue), having $v_z > 0$ are shown to illustrate their different orbital phases. The shaded region around NGC 3201's orbit shows 100 orbits that were randomly sampled with errors in observations, which were integrated for 1.5 Gyr. It aligns with the orbit of ED-3 stars after multiple revolutions. Brown points show the Gjöll stream, overlapping with NGC 3201's trailing orbit, green arrow indicates NGC 3201's velocity direction. Reproduced from Dodd et al. [2024].

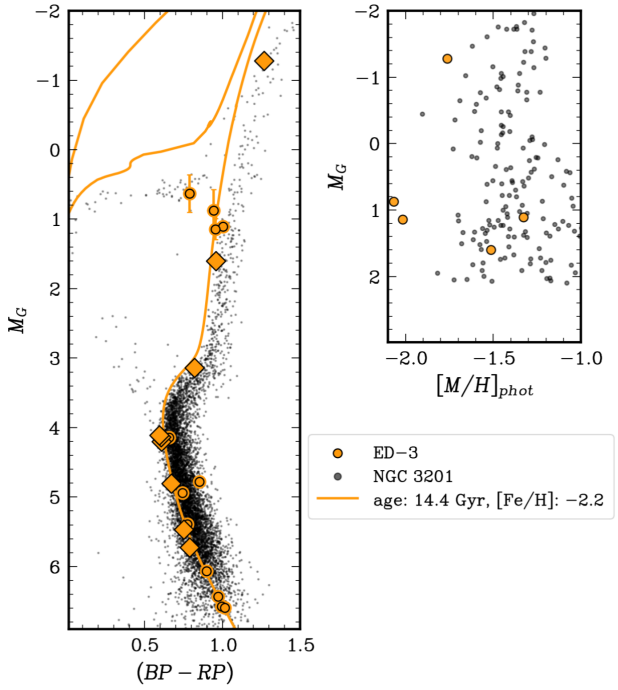

Figure 6: The left panel of Figure 6.12 from Dodd et al. [2024] shows the CMD of ED-3 (orange) and NGC 3201 stars (black), while the right panel displays photometric metallicities from Andrae et al. [2023]. Some ED-3 stars have similar metallicities to NGC 3201, and two RGB stars show consistent [Fe/H] values within 0.1 dex. Reproduced from Dodd et al. [2024]

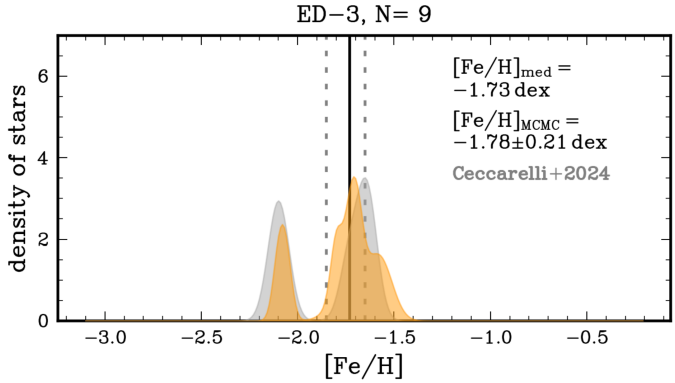

Figure 7: Normalized metallicity distributions of ED-3 from Fe II lines, reporting the median metallicity, mean [Fe/H], and intrinsic dispersion. Reproduced from Dodd et al. [2024].

2 Methodology

2.1 Short description

The goal of this project is to establish the existence of a link between NGC 3201 and ED-3. For this purpose, initial conditions for a dwarf galaxy-like system that could represent ED-3 will be created, in order to perform forward integrations in time to deduce if recreating ED-3 and NGC 3201 kinematics is possible. We will integrate orbits for three timespans namely, 5 Gyr, 7.5 Gyr and 10 Gyr and we will consider 3 different masses, 5 x 10^6 $M_\odot$, 10^6 $M_\odot$ and 5 x 10^5 $M_\odot$, and 2 different sizes (20 pc and 250 pc) of the progenitor of ED-3. We will then investigate the most fitting integration time and mass for the simulation of the progenitor star cluster that mimics best ED-3 and, if possible, NGC 3201 motion and positions simultaneously. For each of these cases the process will be the same, we run orbit integrations of different initial conditions. The dwarf is composed of 10^4 particles and is embedded within a Milky Way potential. We place the progenitor of ED-3 on the same orbit and integrate forward in time. AGAMA (Action-based Galaxy Modelling Architecture) is used throughout, due to its versatility for stellar and galactic modelling [Vasiliev, 2019].

2.2 Initial properties: ED-3 progenitor

To set the size and mass of the progenitor of ED-3, we use the mass-metalicity relation described in Kirby et al. [2013],

$$\langle [\mathrm{Fe/H}] \rangle = (-1.69) + (0.30) \log \left(\frac{M_*}{10^6 M_\odot} \right). \tag{1}$$

Since ED-3's median metalicity is equal to -1.73 dex, see Figure 7, it implies a mass of approximately 10^6 $M_\odot$ for the system.

Following this, we can set the radius of the system, for which we use the observed M_V - $r_{1/2}$ relation from Tolstoy et al. [2009]. We assume the progenitor to be a Local Group Dwarf, identified by the open blue and green pentagons in Figure 8.

Given the ratio $\frac{M_*}{L_*} = 2.5$, as referenced in Armandroff and Da Costa [1986], the luminosity of a system of $10^6 M_\odot$ will be 4 x $10^5 L_\odot$. Using the relation between absolute magnitude and luminosity,

$$M_V = M_{V,\odot} - 2.5 \log_{10} \left(\frac{L_V}{L_\odot} \right), \tag{2}$$

this results in an approximate M_V = -9. Figure 8 shows that this V-band magnitude corresponds to the faint tail end of dwarf galaxies and yields a value of $\log(r_{1/2}) = 2.4$, resulting in a scale radius of 0.25 kpc for the progenitor. We have also considered a system of a radius of 20 pc, which would represent a massive extended star cluster, therefore located close to NGC 2419 in Figure 8.

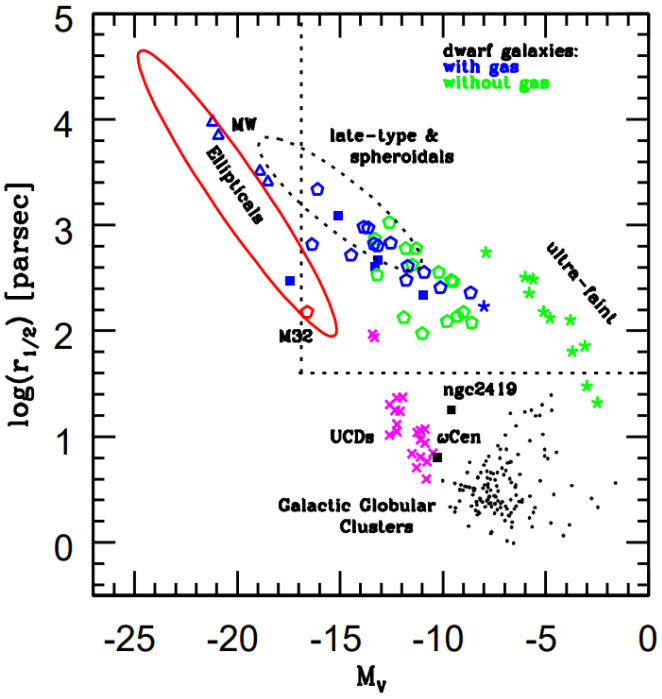

Figure 8: Relationship between structural properties of Local Group dwarf galaxies and other objects: M_V against half-light radius ($r_{1/2}$). Local Group dwarf galaxies are represented as open pentagons, with blue indicating systems containing gas and green for systems without gas. Reproduced from Tolstoy et al. [2009]

2.3 AGAMA

AGAMA (Action-based Galaxy Modelling Architecture) provides advanced tools for orbit integration and modeling gravitational potentials, essential for studying stellar dynamics and galaxy evolution. Its high-accuracy numerical integrators allow precise orbit computations in both static and time-dependent potentials, enabling the modeling of dynamic systems. AGAMA supports a wide range of potential functions, including spherical models (e.g., Plummer [Plummer, 1911] and Hernquist [Hernquist, 1990]), axisymmetric and triaxial forms (e.g., Miyamoto-Nagai[Miyamoto and Nagai, 1975]), and composite potentials that combine multiple components such as disk, bulge, and halo for realistic galaxy simulations. AGAMA's orbit libraries and customizable routines are ideal for constructing phase-space structures such as tidal streams [Vasiliev, 2019].

For the MW potential, we will be using the McMillan potential (from McMillan [2017]). This potential is composed of multiple components: $\Phi_{\text{bulge}}, \Phi_{\text{thin disk}}$, $\Phi_{\text{thick disk}}, \Phi_{\text{HI gas disk}}, \Phi_{\text{HII gas disk}}, \Phi_{\text{dark matter}}$ as seen in McMillan [2017]. In the initialization of AGAMA, `agama.setUnits(mass=1, length=1, velocity=1)` was used to instruct the library to take Galactic units as standard, meaning the values are 1 $M_\odot$, 1 kpc and 1 km/s.

To generate a progenitor for ED-3, we also use AGAMA. We assume the system follows a Plummer profile, inserted into the MW potential, that follows the distribution,

$$\Phi(r) = -\frac{GM}{\sqrt{r^2 + a^2}} \tag{3}$$

where a is the scale radius, for a simplified, spherically symmetric potential. The self-consistent Plummer model has an associated distribution function (DF) from which the velocities are determined. In the case of a Plummer model with a scale radius of 0.25 kpc and a total mass of 5 x 10^6 $M_\odot$ the total velocity dispersion is $\sigma_v = 5.03$ km/s ($\sigma_x, \sigma_y, \sigma_z = 2.91$ km/s). For the model with a scale radius of 0.02 kpc and the same mass, the total velocity dispersion is $\sigma_v = 17.78$ km/s ($\sigma_x = 10.31, \sigma_y = 10.18, \sigma_z = 10.29$ km/s). Using the DF, AGAMA creates an object from which 10^4 particles are sampled, simulating positions and velocities for the progenitor. The dataset is centered on the progenitor, and Figure 9 histograms of the spatial and velocity distributions of the initial configuration.

In practice, to draw a distribution function from the given potential, the class `agama.DistributionFunction` is used. Class `agama.GalaxyModel(pot, df)` allows for creation of a galactic type object, according to the input potential and distribution function, allowing for 6D spatial and velocity coordinates to be extracted. In this case, the variables are Plummer potential and Quasispherical distribution. The function `gm.sample (N_particles)` returns two arrays, one Nx6 array of positions and velocities, followed by a 1D, N length array of individual masses for each point source in the simulation.

2.4 Backwards orbit integration

The starting point is creating a backwards trial orbit of a single star and for simplicity and for testing purposes we use the Sun. Once the orbit has been computed backward in time, the last coordinates are used as a starting point for a forward integration back to present time. This is done by creating a function `orbint`, that takes as input the initial 6D conditions, the total integration time, and time steps. The orbit data results come in the form of a 6D array, 3 coordinates for position and 3 for velocity, and they are visualized in multiple projections (*x*-*y*, *x*-*z*, *y*-*z*, and *R*-*z* planes). Following this, the ED-3 dataset [Dodd et al., 2023] is loaded and run through the same process as before, integrating backward in time and forward, in order to map the path of the 16 stars, observe patterns and possible deviations from the initial expectations. Once the trial method is validated and considered robust, the next step is to transform NGC 3201's coordinates [Baumgardt, Accessed 2025] from the ICRS to the Galactocentric frame, using `astropy.coordinates.SkyCoord`, for compliance with the ED-3 dataset [Dodd et al., 2023].

Initially, the chosen point to center the progenitor was on the orbit of NGC 3201, but as we shall see in the next section, once the simulation was completed, the results were suboptimal. Therefore, the decision was made to change the approach and center the distribution on one of the ED-3 stars located in a more densely populated area, in terms of its other members. In this case, the choice was made for the ED-3 star index 4, referred to as ED-3-4 hereafter. The distribution is then shifted to the backward integrated coordinates of this star, for centering on ED-3-4, at 10 Gyr, 7.5 Gyr, or 5 Gyr back in time.

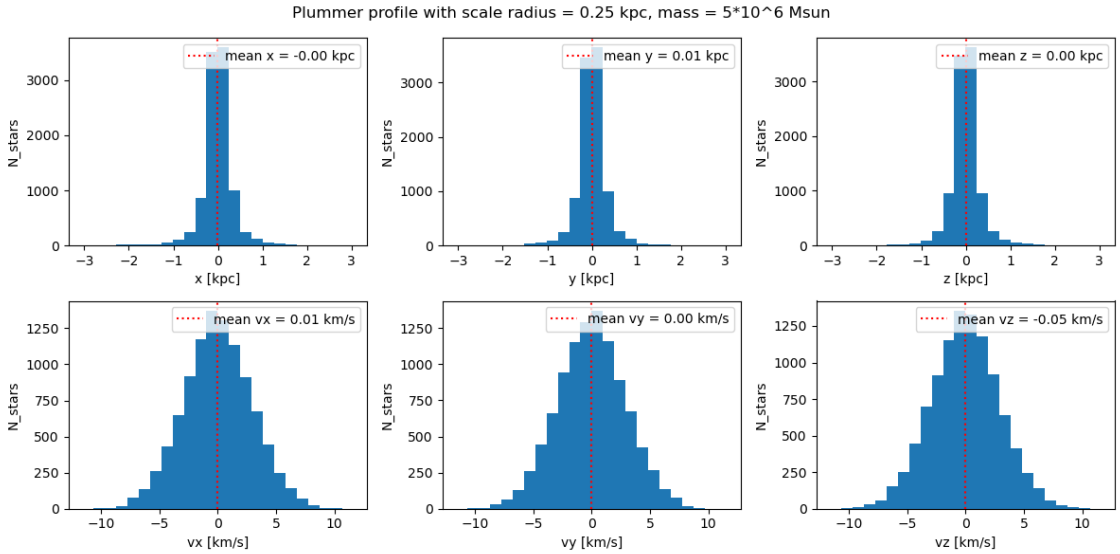

Figure 9: Initial distribution of the simulated dwarf containing 10^4 particles of the same mass. This representation shows the unshifted coordinates for the distribution in 6D space.

2.5 Angular Momentum and Energy

Given that the ED-3 substructure was identified as a clump in IoM space, we compute the angular momentum and energy for every particle of the simulated system to further analyze its properties in connection to NGC 3201 and their possible common progeny. Using `np.column_stack` to compute the position and velocity array (uncorrelated for simplicity) vectors, the angular momentum (including the perpendicular component) is calculated using the cross product of position array `r` and velocity array `v`. Then it is split into it's (x, y, z) components, along with the perpendicular angular momentum component, according to these formulas,

$$\mathbf{L} = \mathbf{r} \times \mathbf{v} \tag{4}$$

$$\mathbf{L} = (L_x, L_y, L_z) \tag{5}$$

$$L_\perp = \sqrt{L_x^2 + L_y^2}. \tag{6}$$

To compute the potential energy, the AGAMA potential function, `p.potential(positions)` is used, with `p` representing the Galactic potential and `positions` being the positions at present time for all sources in x, y, z coordinates. Kinetic energy is calculated using the function,

$$KE = \frac{1}{2}v^2, \tag{7}$$

that takes as variable the 3D velocity array of each object.

Scatter plots with errors for ED-3 are made for three representations, namely, E-L_z, L_{perp}-L_z, E-L_{perp}. By convention, the sign of the angular momentum was flipped, such that prograde orbits have $L_z > 0$.

3 Analysis

Previous work has explored the association between globular clusters and streams (see Chang et al. [2020]), although not for ED-3 and NGC 3201. Here we will analyze and discuss different time periods of integration and different masses for the progenitor of ED-3, in order to determine the timeline of accretion into the Milky Way.

Two different centering points were used for the orbit integration process namely, NGC 3201 and star ED-3-4. These cases will be evaluated in order to determine the best overlap between the simulated points and observed data (ED-3 and NGC 3201). Each of the cases will be illustrated using two phase space plots showing positions and velocities (see Figures 10 and 12 for examples). The observed ED-3 stars split into two groups with positive and negative v_z velocities, with a ratio of $N(v_z > 0)/N(v_z < 0) = 7$. All of the ED-3 substructure members have negative v_y, with most stars having positive v_x. All plots shown are in Galactocentric Cartesian coordinates. In all figures, grey points are the simulated particles, orange points correspond to the candidates within a radius of 2.45 kpc from the Sun (solar neighborhood), green points show the ED-3 stars, and the red star represents NGC 3201.

3.1 NGC 3201 centering

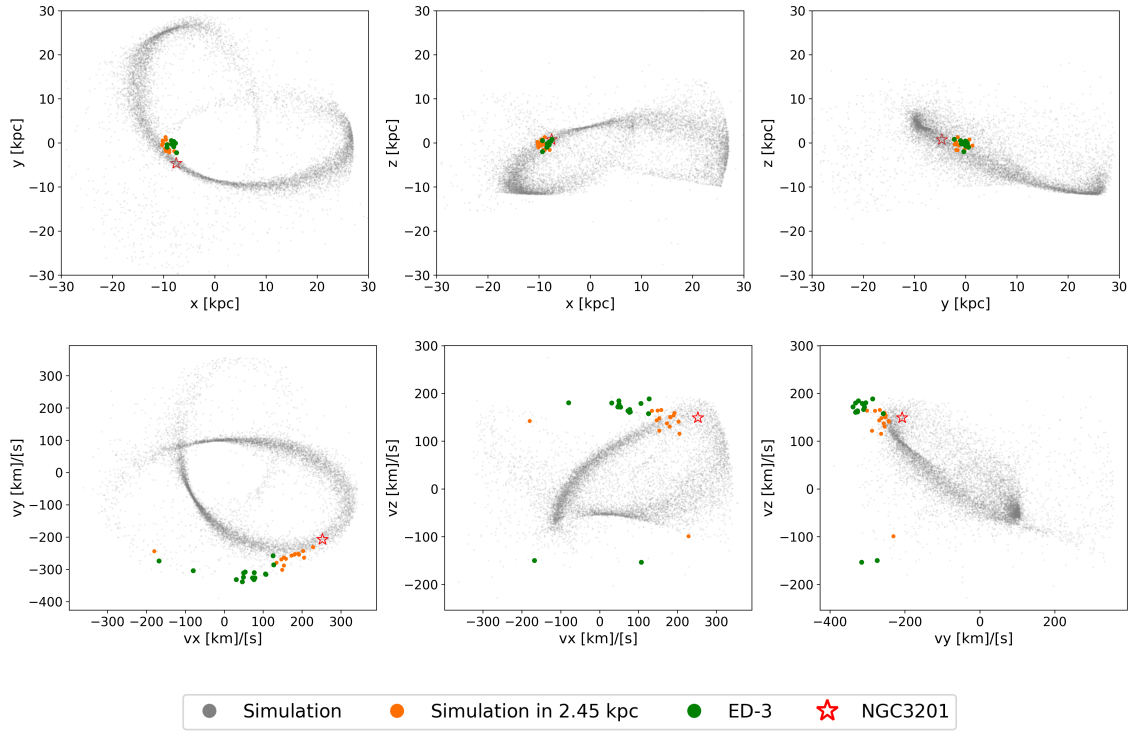

Figure 10: Results of the integration of a system of $r = 0.25$ kpc, mass 5 x 10^6 $M_\odot$ for a period of 5 Gyr, centered on the orbit of NGC 3201. Top panels - positions, bottom panel - velocities.

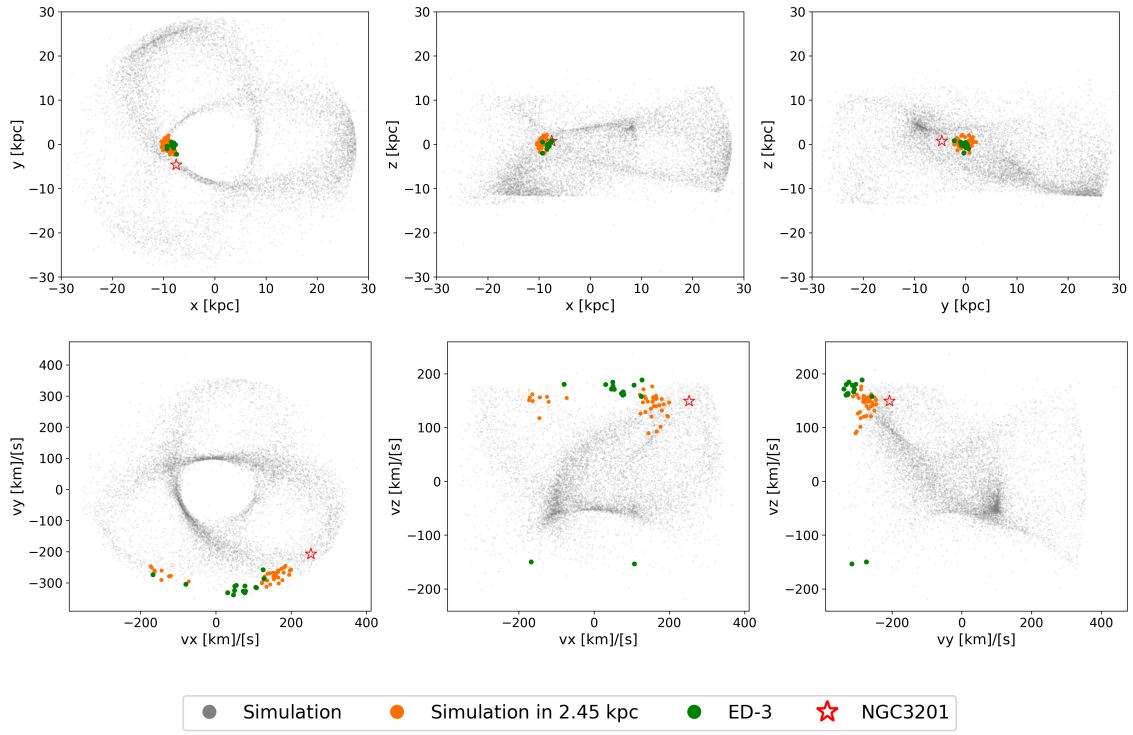

Figure 11: Results of the integration of a system of $r = 0.25$ kpc, mass 5 x 10^6 $M_\odot$ for a period of 10 Gyr, centered on the orbit of NGC 3201. Top panels - positions, bottom panel - velocities.

We first analyze the results of centering the progenitor of ED-3 on the orbit of NGC 3201. Apparent in the top panels of all the following figures showing positions is the small volume that the ED-3 points are constrained in, which reflects that all ED-3 stars are located within 2.45 kpc from the Sun (solar neighborhood).

Firstly, the 5 x 10^6 $M_\odot$ and 5 Gyr case of Figure 10 reveals that while there are some candidates within the solar neighborhood, this integration time is too short to provide enough mixing and spread of simulated points for a reasonable number of stars to lie within the specified radius represented by the orange points. Secondly, the NGC 3201 centering does not result in good overlap with the ED-3 stars (green points) in the x-y plane of the positions plot. The stream-like structure has negative offset in v_z compared to ED-3 members, such that only part of the stream overlaps with the solar neighborhood, and consequently ED-3. Although the overlaps in the x-z and y-z plane appear reasonable considering the location of the main stream that was simulated, the velocity plot associated provides further information on the incompatibility of this centering.

The bottom panels of Figure 10 reveal an almost non-existent overlap in all three velocity projections, with all the candidates (orange points) being found offset from the ED-3 member stars. Also, no simulated points are found with very large and negative v_z, the only candidate being at $v_z = -100$ km/s, whereas there are 2 ED-3 stars with $v_z =$ ˜-150 km/s.

The case of NGC 3201 centering with 10 Gyr integration period and 5 x 10^6 $M_\odot$ is shown in Figure 11. Although this case shows a small but reasonable number of simulated candidates within the 2.45 kpc volume from the Sun, the velocity space projections of Figure 11 show that the observed ED-3 members have more negative v_y velocities than the counterparts in the simulations. Furthermore, their positive v_z are higher, while there are no simulated particles with negative v_z values present in this case. Also, Figures 10 and 11 show that simulated particles are never able to match ED-3's $v_x < 0$ component either.

Despite the negative results, a conclusion that can be drawn from this section is that the 5 *Gyr* orbit integration period is inadequate for this study, due to the insufficient mixing and spread of the simulated points in the given timespan. This leads to a mostly single stream-like structure, which does not overlap with the locations in phase space of the ED-3 group, not in $v_z > 0$, nor in $v_z < 0$. In comparison, the higher integration time and mass case shows a much more reasonable spread and mixing of points, for the purposes of this study. Therefore, the 5 Gyr case will not be taken into account in the work that follows.

3.2 ED-3 Centering with $r_{1/2} = 0.25$ kpc

In this section, we will explore the results obtained from centering the progenitor on ED-3-4's orbit.

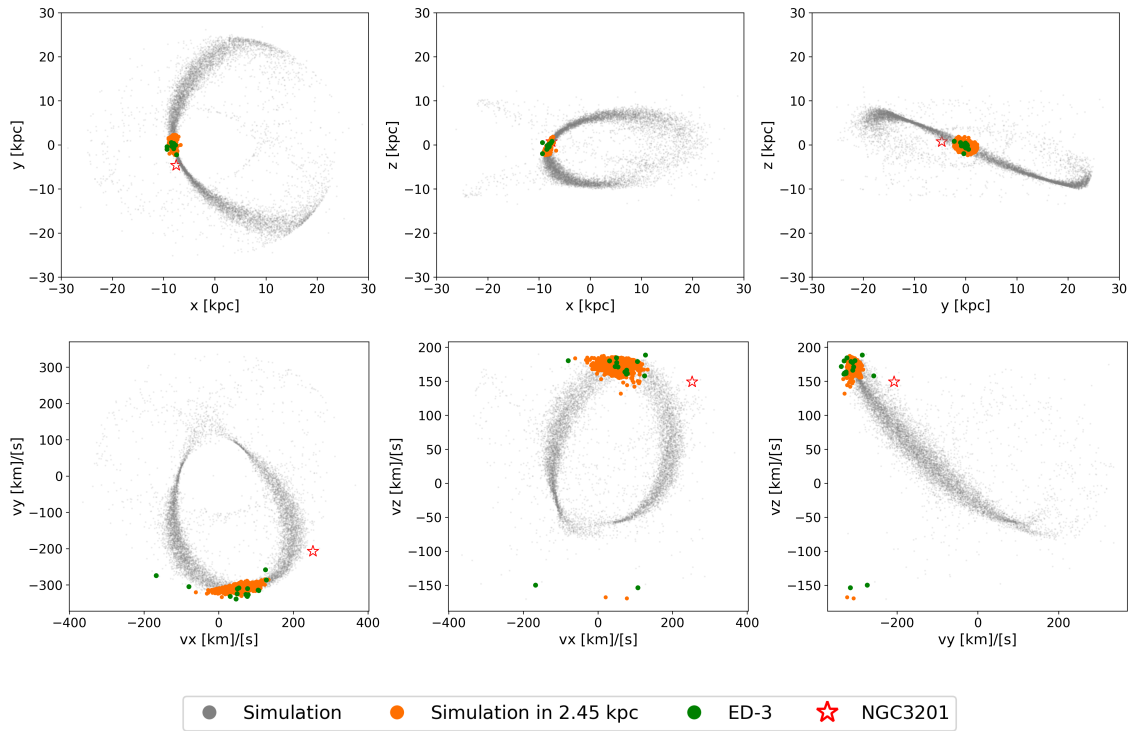

Figure 12: Results of the integration of a system of $r = 0.25$ kpc, mass 5 x 10^5 $M_\odot$ for a period of 7.5 Gyr, centered on the orbit of ED-3-4. Top panels - positions, bottom panel - velocities.

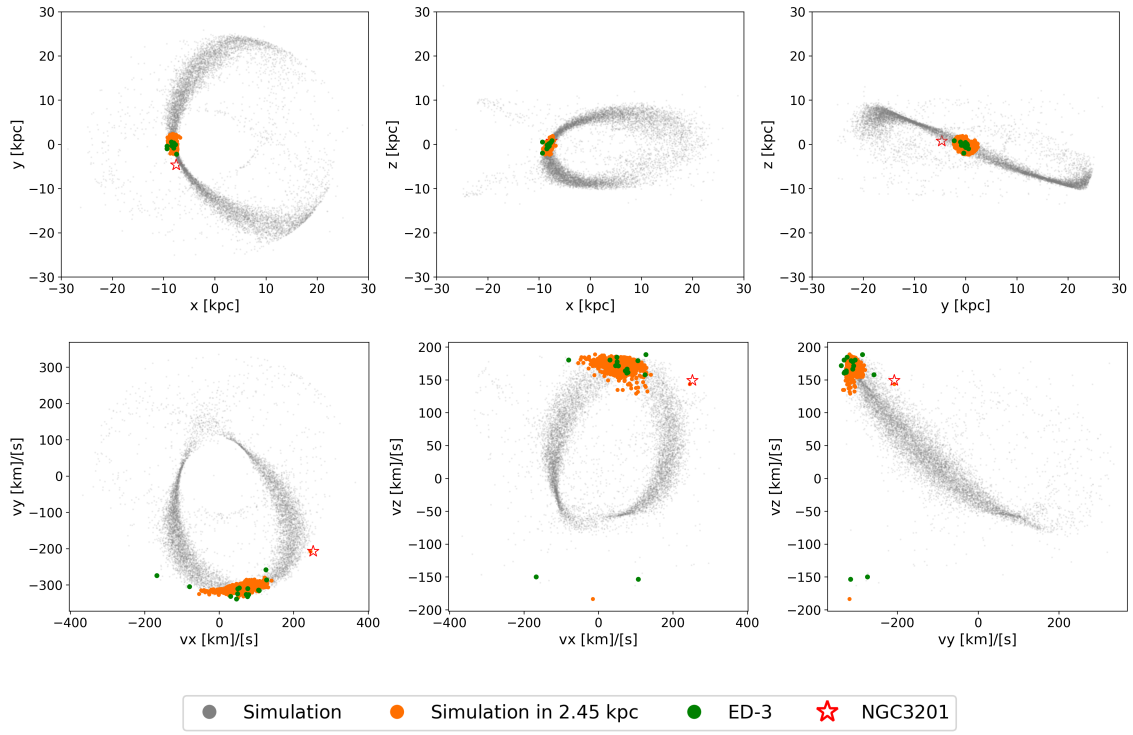

Figure 13: Results of the integration of a system of $r = 0.25$ kpc, mass 10^6 $M_\odot$ for a period of 7.5 Gyr, centered on the orbit of ED-3-4. Top panels - positions, bottom panel - velocities.

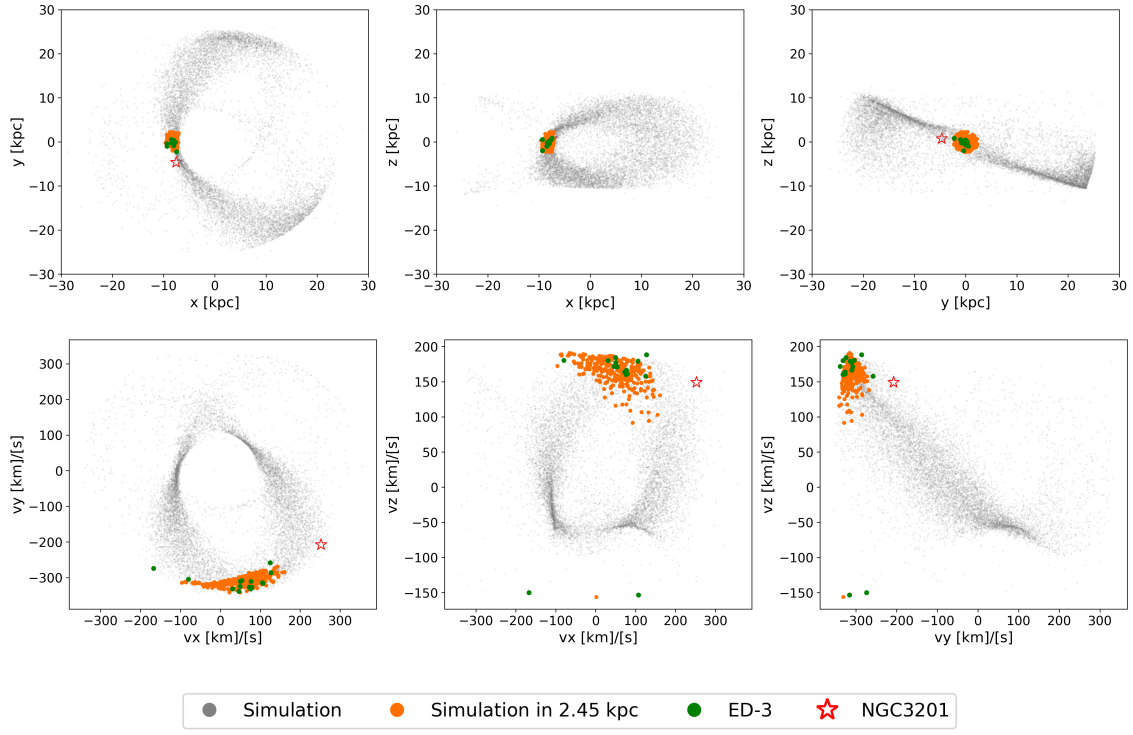

Figure 14: Results of the integration of a system of $r = 0.25$ kpc, mass 5 x 10^6 $M_\odot$ for a period of 7.5 Gyr, centered on the orbit of ED-3-4. Top panels - positions, bottom panel - velocities.

For the case with a scale radius of $r = 0.25$ kpc and 7.5 Gyr integration period, we show three different masses for the system, 5 x 10^5 $M_\odot$ (Figure 12), 10^6 $M_\odot$ (Figure 13) and 5 x 10^6 $M_\odot$ (Figure 14). All three cases present very similar characteristics, the stream structure is clearly visible, both in position and velocity space, indicating a lack of mixing and spread of simulated particles. However, they show a longer stream structure and higher diffusion (width of stream) than in the 5 Gyr case shown for NGC 3201. This is further accentuated by the near absence of candidate stars (orange) in the negative v_z area of velocity space, where only one or two simulated particles are found, respectively, with a similar trend for the most negative v_x stars, not being reproduced. Therefore, a 10 Gyr integration period will be inspected.

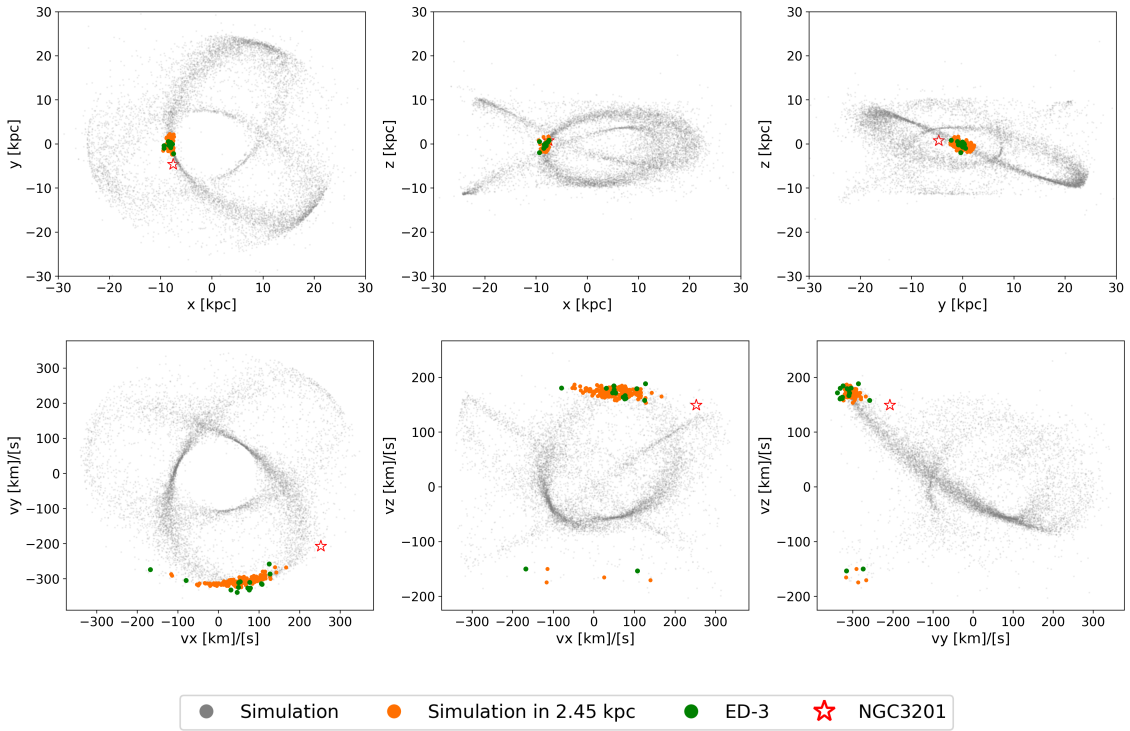

Figure 15: Results of the integration of a system of $r = 0.25$ kpc, mass 5 x 10^5 $M_\odot$ for a period of 10 Gyr, centered on the orbit of ED-3-4. Top panels - positions, bottom panel - velocities.

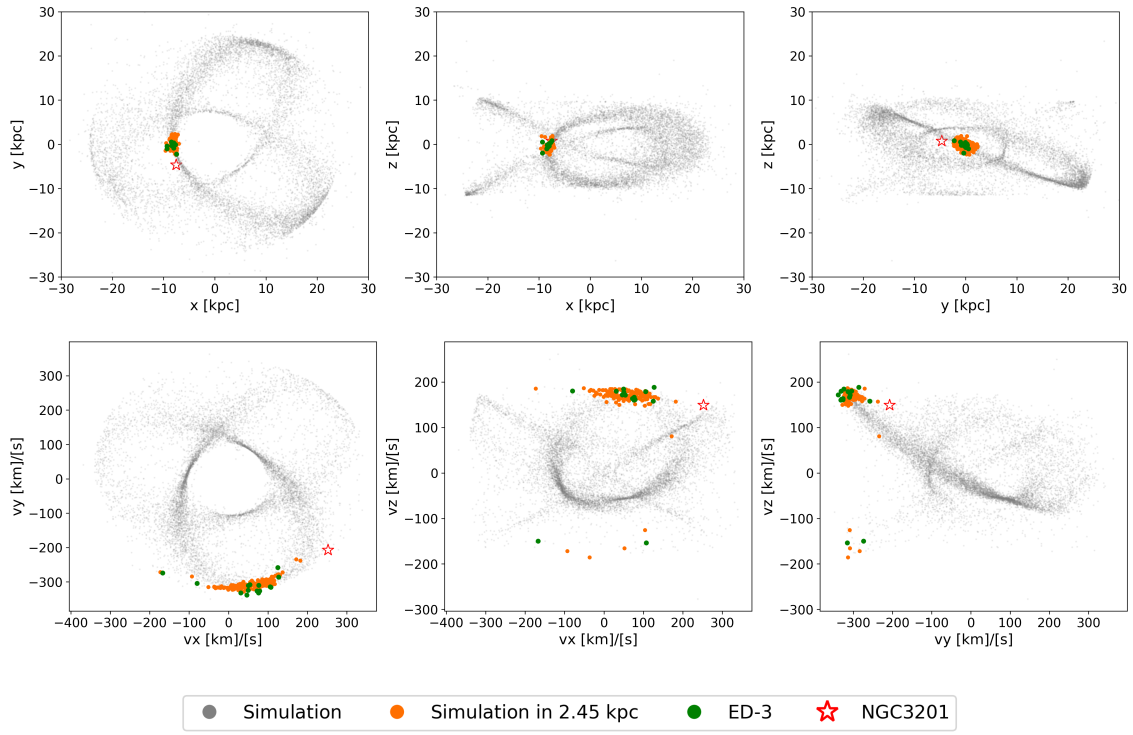

Figure 16: Results of the integration of a system of $r = 0.25$ kpc, mass 10^6 $M_\odot$ for a period of 10 Gyr, centered on the orbit of ED-3-4. Top panels - positions, bottom panel - velocities.

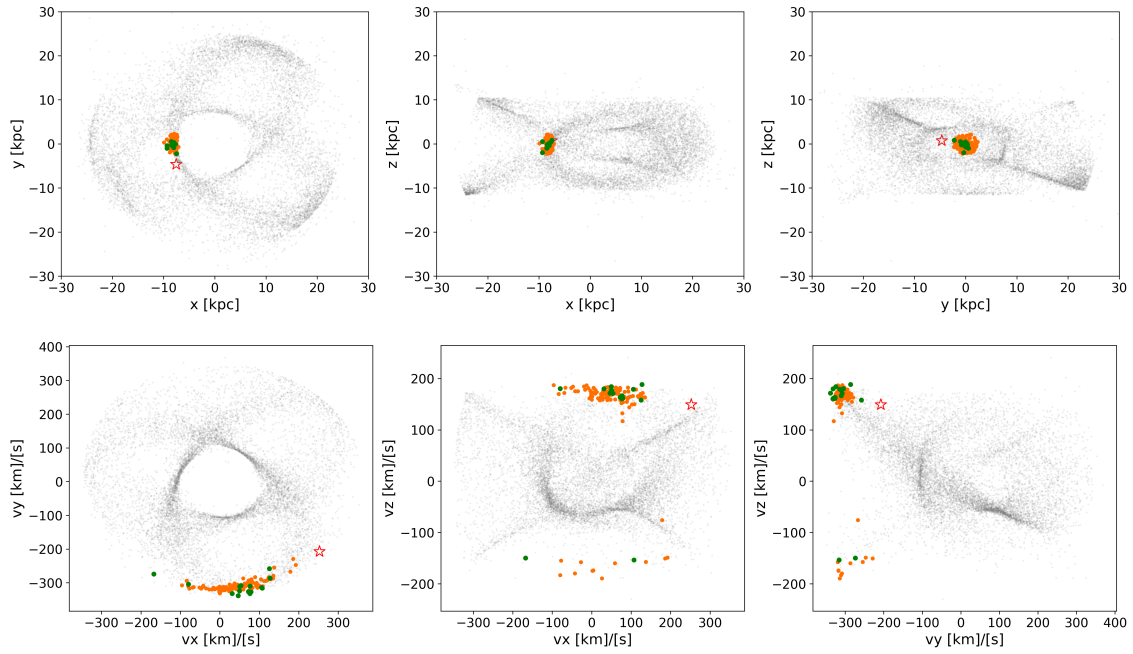

Figure 17: Results of the integration of a system of $r = 0.25$ kpc, mass 5 x 10^6 $M_\odot$ for a period of 10 Gyr, centered on the orbit of ED-3-4. Top panels - positions, bottom panel - velocities.

In the case of a 10 Gyr integration time span, the results are improved for all masses considered. All three masses yield good agreement, as can be seen in Figures 15, 16, 17. The main difference between these results and those presented earlier in this section is the number of candidates in the $v_z < 0$ area, and consequently the degree of phase mixing. When using a 10 Gyr integration period we are able to reproduce the data. The lower mass progenitors, shown in Figure 15, 16, each indicate four possible candidates, with $v_z < 0$ within the $r = 2.45$ kpc solar neighborhood and $N(v_z > 0)_{sim}/N(v_z < 0)_{sim} = 40$ for both, whilst the largest shows twelve candidates with $N(v_z > 0)_{sim}/N(v_z < 0)_{sim} = 8.75$. Stream-like structures can still be observed in all three cases, but the spread and mixing of simulated points is vastly improved from previous integration periods, especially in the most massive system, as expected from the relation between integration time to degree of phase mixing and diffusion discussed in Koppelman et al. [2018]. Alongside this, the number of wraps of the simulation is increased, demonstrated by the almost disk-like shape of the particles in the x-y position panel in Figure 17, as well as the diffusion of the streams, indicating slightly better mixing.

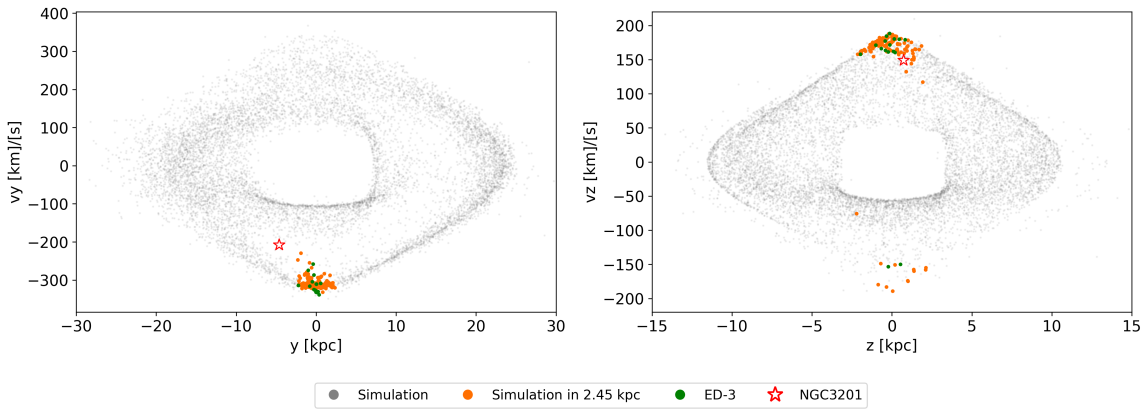

Figure 18: Projections in y-vy, z-vz space of the $r = 0.25$ kpc, 5 x 10^6 $M_\odot$, 10 Gyr case.

The 10 Gyr integration time with a mass of 5 x 10^6 $M_\odot$ seems to reproduce the ED-3 data the best for the ratio $N(v_z > 0)_{sim}/N(v_z < 0)_{sim} = 8.75$. To further emphasize this decision, a plot of y-vy, z-vz projections has been computed in Figure 18. Grey points represent all particles of the progenitor system, orange points are the candidates within the 2.45 kpc local volume of the progenitor, green points show ED-3 stars and the red star symbol is NGC 3201. The left panel shows that the globular cluster as being separated from the group of ED-3 and candidates, while the left panel showcases the separation between the main $v_z > 0$ group and the $v_z < 0$ area. In the latter panel, the 2 ED-3 member stars are observed to be in close proximity to the negative v_z candidates, the rest being more negatively offset in v_z.

3.3 ED-3 centering with $r_{1/2} = 0.02$ kpc

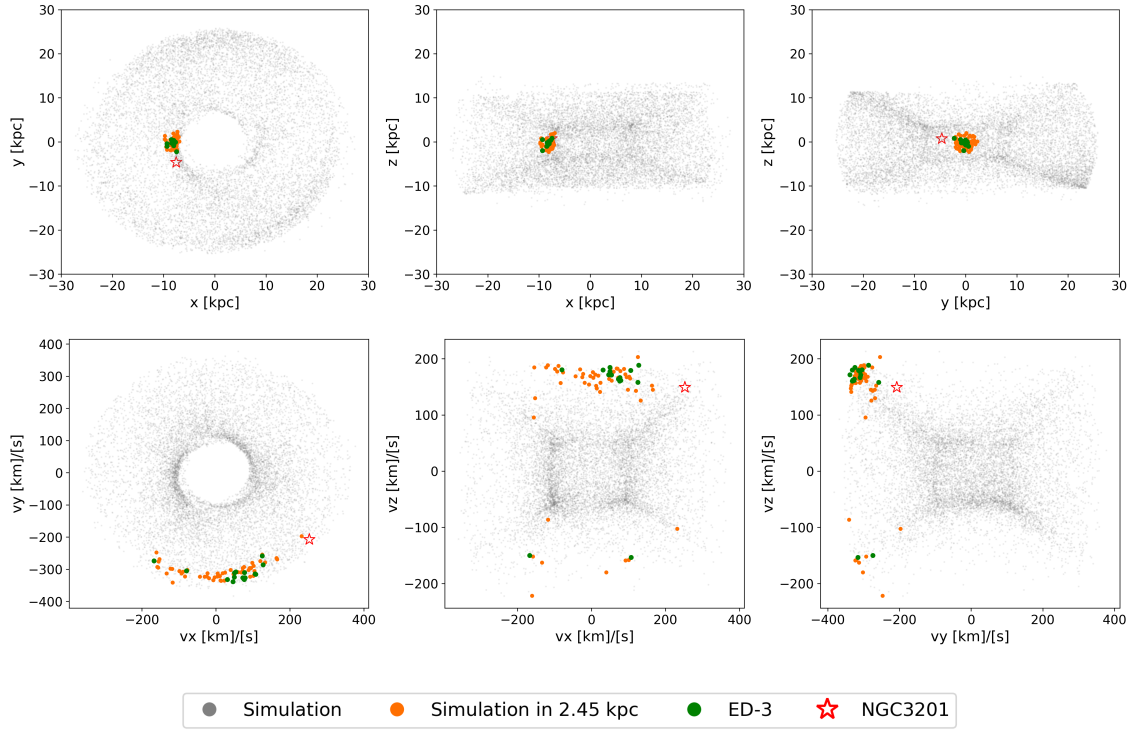

Figure 19: Results of the integration of a system with $r_{1/2} = 0.02$ kpc of mass 5 x 10^6 $M_\odot$ for a period of 7.5 Gyr, centered on the orbit of ED-3-4. Top panels - positions, bottom panel - velocities.

We therefore also investigated a progenitor with a scale radius of 20 pc (massive GC), and a mass of 5 x 10^6 $M_\odot$. We show the results of integrating for 7.5 and 10 Gyr (Figures 19, 20), yielding a good mixing in all panels of the two figures. The 7.5 Gyr case shows a very good overlap in both $v_z > 0$ and $v_z < 0$ with a ratio of $N(v_z > 0)_{sim}/N(v_z < 0)_{sim} = 5.75$, with simulated particles close to both ED-3 stars. The 10 Gyr option, although less simulated particles overlap with ED-3 in the positive v_z area, shows a greater number of candidates for the $v_z < 0$ ED-3 group, having a ratio of $N(v_z > 0)_{sim}/N(v_z < 0)_{sim} = 1.82$. While maintaining the same mass and integration time conditions as previous results from Section 3.2, the smaller scale radius of 0.02 kpc allows for more mixing in both position and velocity space. This is evidenced by the more diffuse stream-like structures seen in the panels of the phase-space plots.

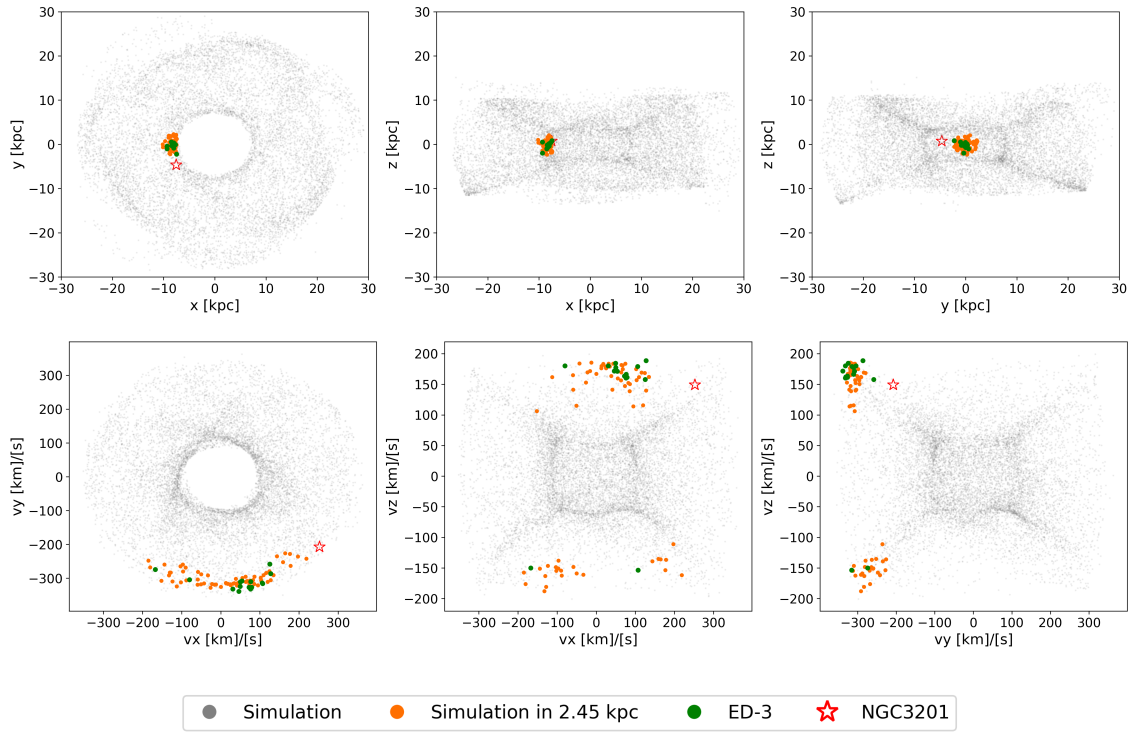

Figure 20: Results of the integration of a system with $r_{1/2} = 0.02$ kpc of mass 5 x 10^6 $M_\odot$ for a period of 10 Gyr, centered on the orbit of ED-3-4. Top panels - positions, bottom panel - velocities.

3.4 Distribution in IoM

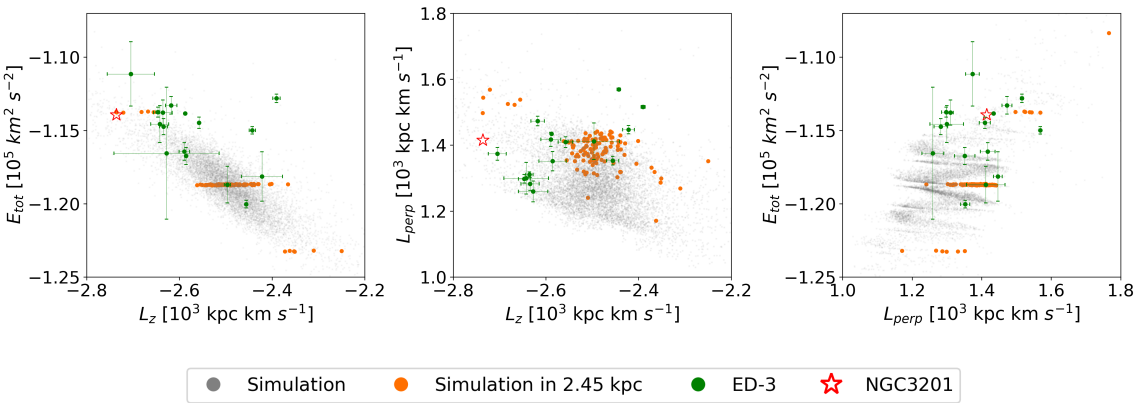

Figure 21: IoM of ED-3, NGC 3201 and simulation: $r = 0.25$ kpc, 10 Gyr - 5 x 10^6 $M_\odot$. Orange - simulated stars with a local volume of $r = 2.45$ kpc, green - ED-3, red star - NGC 3201. Error bars are shown for ED-3 in all three projections.

Ancient accretion events can be detected through the leftovers of their progenitors (debris) by observing clumps in the IoM. The advantage of using IoM is that all the wraps in phase space fold over effectively into a single structure in the IoM. NGC 3201 and ED-3 are very close in this space, as is illustrated in Figure 3.

We build on these results by focusing only on these two objects, offering a zoomed in view of their properties, including errors in all three coordinates, presented in Figure 21. This Figure also shows the particles for the most massive case in this study ($r = 0.25$ kpc). Similar structures are observed in the first and last panel, namely the lines formed by local volume stars at approximately $E_{tot} = -1.19$ x 10^5 km^2 s^{-2} and ranges of $-2.6 < L_z < -2.35$ x 10^3 kpc km s^{-1} and $-1.45 < L_{perp} < -1.25$ x 10^3 kpc km s^{-1}. Each of these lines are representations in IoM space of different stellar streams moving in different directions, with respect to each other. The error bars of ED-3 bring certain stars within very close range of each other, indicating the possibility of similar structures to the lines described earlier, particularly in the $E_{tot} - L_z$ and $E_{tot} - L_{perp}$ plots. Tightness can be observed in all three projections, indicating a fairly strong connection between ED-3 and NGC 3201, as well as a reasonable reproduction of these two using the simulated candidates, considering the proximity of orange points to the globular cluster and ED-3. The range of values for L_z and L_{perp} are consistent with results from Dodd et al. [2024] and Dodd et al. [2023].

3.5 Is there a link between ED-3 and NGC 3201?

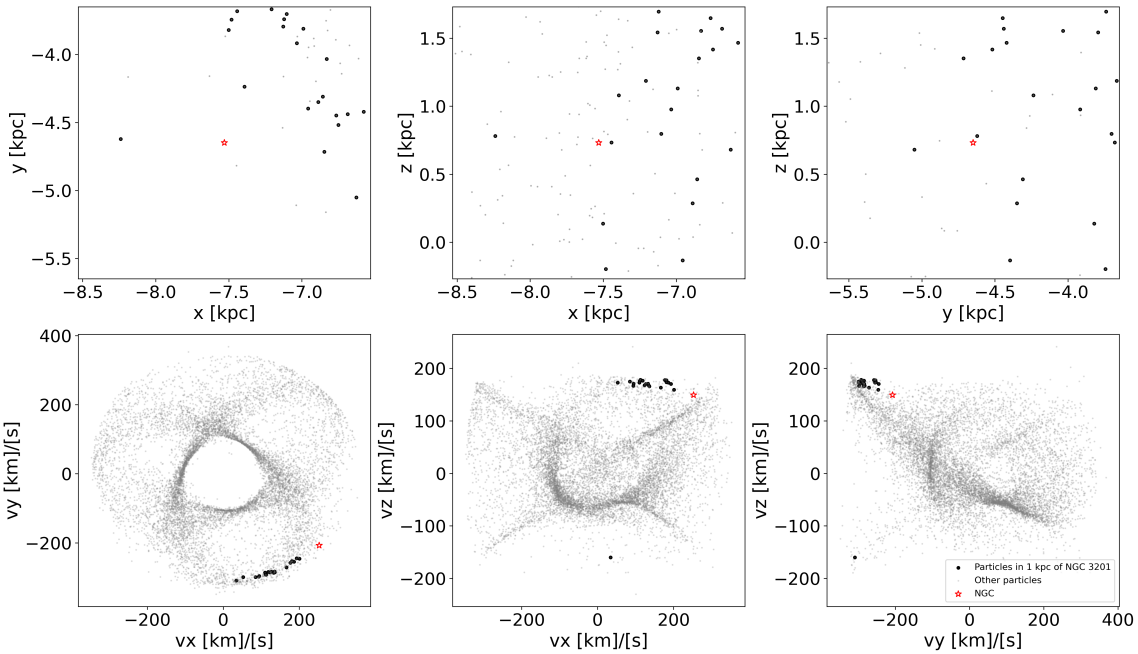

Figure 22: Overlap candidates in positions, with velocity correspondence: $r = 0.02$ kpc, 10 Gyr - 5 x 10^6 $M_\odot$.

To discern whether or not NGC 3201 and ED-3 could be associated, we determine whether any of its simulated particles have phase-space coordinates similar to those of the progenitor of ED-3. Therefore, figures similar to the previous ones is made, except this case gives a zoomed-in view of the positions of simulated particles close to the globular cluster. This is shown in Figure 22. In the upper panels of Figure 22, only particles within 1 kpc from the coordinates of NGC 3201 in all directions are shown. In the bottom panels

of Figure 22, the candidates identified previously are plotted in velocity space to relay information about their connection with NGC 3201. We note the lack of overlap with NGC 3201 in the velocity panels. Due to there being no candidates in NGC 3201's immediate vicinity, it is unclear whether ED-3 and NGC 3201 originate from the same progenitor with a mass of 5 x 10^6 $M_\odot$ and 10 Gyr integration time.

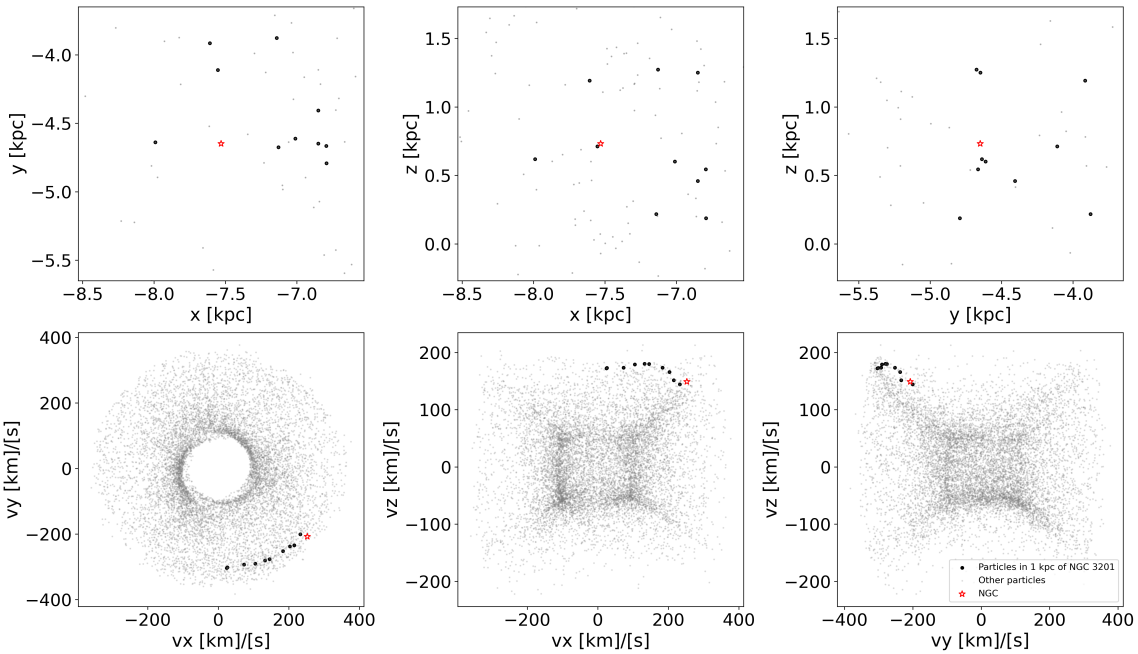

Figure 23: Overlap candidates in positions, with velocity correspondence: $r = 0.02$ kpc, 7.5 Gyr - 5 x 10^6 $M_\odot$.

We also further analyze the option of a $r = 0.02$ kpc, 7.5 Gyr and 5 x 10^6 $M_\odot$ (massive GC) progenitor in the same fashion. Even though this case has a ratio of $N(v_z > 0)_{sim}/N(v_z < 0)_{sim} = 5.75$, further from the ED-3 ratio than the dwarf progenitor case, it does show closer candidates in the velocity space panels of Figure 23, compared to Figure 22.

For both progenitor cases, simulated particles are found in the 1 kpc volume of NGC 3201. Their velocity space distances are 11.83 km/s for the dwarf galaxy progenitor and 15.85 km/s in the case of the massive globular cluster. NGC 3201's velocity errors are relatively small, with values of $d_{(v_x)}$ = 1.50, $d_{(v_y)}$ = 0.28 and $d_{(v_z)}$ = 0.58 km/s. Therefore, the previously mentioned particles do not reside within the volume given by the errors in velocity, although considering the small difference in velocity, it remains a possibility that either of these particles can reproduce NGC 3201.

4 Conclusion

Given the proximity in integrals of motion space and similar orbits of ED-3 and NGC 3201, [Dodd et al., 2024] suggested that these two structures might be connected. A quantitative method was developed to analyze their possible connection. Starting from initial conditions of ED-3-like progenitors, orbit integration is performed for progenitors of different masses (5 x 10^5, 10^6, 5 x 10^6 $M_\odot$), integration times (5, 7.5 and 10 Gyr), two radii ($r = 0.25$, $r = 0.0.02$ kpc), and centering points (NGC 3201 and ED-3-4). Velocities are compared with ED-3. Finally, angular momentum and energy plots are analyzed, in combination with ratios ($N(v_z > 0)/N(v_z < 0)$) and distances of closest simulated particles (in position and velocity) to NGC 3201. This is done in order to determine what progenitor conditions, if any, reproduce the observed values of ED-3 and NGC 3201.

Within the limits of the experiment done here, one can conclude that NGC 3201 is not the core of the ED-3 progenitor, as there is insufficient overlap between ED-3 and the simulated particles, as is shown in Section 3.1, Figure 10. To summarize, only the tails of the ED-3 velocity distribution overlap. Therefore, centering on ED-3 stars is considered to be the next best possibility. Star ED-3-4 was selected as it yielded the most overlaping simulated particles with ED-3 data in 6D phase-space and IoM (see Section 3.2).

Inspection of the different cases indicates that an integration time of 10 Gyr, mass of 5 x 10^6 $M_\odot$ and scale radius of $r = 0.25$ kpc is the most fitting reproduction of ED-3 (Figure 17), based on the velocity distribution and ratio of $N(v_z > 0)/N(v_z < 0)$ of the simulated progenitor. This ratio entails $N(v_z > 0)_{sim}/N(v_z < 0)_{sim} = 8.75$, while ED-3's ratio is 7. The second closest option having good overlap in velocity space and $N(v_z > 0)_{sim}/N(v_z < 0)_{sim} = 5.75$, is the 7.5 Gyr, 5 x 10^6 $M_\odot$ case, for a massive GC progenitor (Figure 19).

For both cases, simulated particles in the proximity of NGC 3201 were selected (see Figures 22 and 23). The closest particles are within 1 kpc and $\approx$ 11.83 km/s, 15.85 km/s for the dwarf galaxy and massive GC, respectively. This implies that, within the constraints of this experiment, the connection between NGC 3201 and ED-3 is possible. Furthermore, it is likely that ED-3's progenitor is a dwarf galaxy or massive GC.

Acknowledgements

I extend my sincere gratitude to my supervisors, Amina Helmi and Hanneke Woudenberg. They have helped me tremendously for the completion of this work, ranging from small insights to full lessons. Their patience and passion for the work have inspired me to push myself in order to become a better student. The time and effort they have spent on this project with me is very appreciated and will continue to inspire me in the future.

I also thank Emilia Minut for supporting me through the whole process and allowing me to talk through the mental barriers of such a project. Her words of encouragement have been invaluable and have made a big difference in my outlook for this study.
To my parents, Daniela and Cristian Popp, I thank you for always being by my side and providing constructive feedback on how to handle this thesis. Your help has always been greatly appreciated.

Bibliography

R. Andrae, H.-W. Rix, and V. Chandra. The astrophysical journals. *The Astrophysical Journal*, 267:8, 2023.

Taft E. Armandroff and G. S. Da Costa. The radial velocity, velocity dispersion, and mass-to-light ratio of the sculptor dwarf galaxy. *The Astronomical Journal*, 92(4):777–791, October 1986. doi: 10.1086/114221.

Giuseppina Battaglia, Amina Helmi, Heather Morrison, Paul Harding, Edward W. Olszewski, Mario Mateo, Kenneth C. Freeman, John Norris, and Stephen A. Shectman. The radial velocity dispersion profile of the galactic halo: constraining the density profile of the dark halo of the milky way. *Monthly Notices of the Royal Astronomical Society*, 364(2):433–442, December 2005. doi: 10.1111/j.1365-2966.2005.09367.x.

Holger Baumgardt. Ngc 3201 globular cluster data, Accessed 2025. URL https://people.smp.uq.edu.au/HolgerBaumgardt/globular/fits/ngc3201.html. Online database of globular cluster properties.

Thomas Bensby and Sofia Feltzing. The galactic thin and thick disks in the context of galaxy formation. *Proceedings of the International Astronomical Union*, 5(S265): 300–303, August 2009. ISSN 1743-9221. doi: 10.1017/s1743921310000773. URL http://dx.doi.org/10.1017/S1743921310000773.

J. Bland-Hawthorn and O. Gerhard. The galaxy in context: Structural, kinematic, and integrated properties. *Annual Review of Astronomy and Astrophysics*, 54(1):529–596, 2016. doi: 10.1146/annurev-astro-081915-023441.

A. Bragaglia, E. Carretta, V. D'Orazi, A. Sollima, P. Donati, R. G. Gratton, and S. Lucatello. Ngc 6535: the lowest mass milky way globular cluster with a na-o anti-correlation? - cluster mass and age in the multiple population context. *Astronomy Astrophysics*, 607:A44, 2017. doi: 10.1051/0004-6361/201731526.

CalPoly. Milky way galaxy image. https://evolution.calpoly.edu/milky-way-galaxy, 2025. Accessed: 2025-01-17.

Bradley W. Carroll and Dale A. Ostlie. *An Introduction to Modern Astrophysics*. Cambridge University Press, Cambridge, UK, 2nd edition, 2007.

Jiang Chang, Zhen Yuan, Xiang-Xiang Xue, Iulia T. Simion, Xi Kang, Ting S. Li, Jing-Kun Zhao, and Gang Zhao. Is ngc 5824 the core of the progenitor of the cetus stream? *The Astrophysical Journal*, 905(2):66, 2020. doi: 10.3847/1538-4357/abc8e6.

E. Dodd, T. Matsuno, A. Helmi, E. Balbinot, T. M. Callingham, E. Starkenburg, H. Woudenberg, and T. Ruiz-Lara. Chemical characterisation of small substructures in the local stellar halo. *Expected 2024*, 2024. Chapter 6.

Emma Dodd, Thomas M. Callingham, Amina Helmi, Tadafumi Matsuno, Tomás Ruiz-Lara, Eduardo Balbinot, and Sofie Lövdal. Gaia DR3 view of dynamical substructure in the stellar halo near the Sun. *Astronomy Astrophysics*, 670:L2, 2023. doi: 10.1051/0004-6361/202244546. URL https://www.aanda.org/articles/aa/full_html/2023/02/aa44546-22/aa44546-22.html.

European Space Agency (ESA). Sagittarius collisions trigger star formation in milky way. https://www.esa.int/ESA_Multimedia/Images/2020/05/Sagittarius_collisions_trigger_star_formation_in_Milky_Way, 2020. Accessed: 2025-01-19.

D. A. Forbes and T. Bridges. Accreted versus in situ milky way globular clusters. *Monthly Notices of the Royal Astronomical Society*, 404(3):1203–1214, 2010. doi: 10.1111/j.1365-2966.2010.16373.x.

T. T. Hansen, A. H. Riley, L. E. Strigari, J. L. Marshall, P. S. Ferguson, J. Zepeda, and C. Sneden. A Chemo-dynamical Link between the Gjöll Stream and NGC 3201. , 901 (1):23, September 2020. doi: 10.3847/1538-4357/ababa5.

William E. Harris. A new catalog of globular clusters in the milky way, 2010. URL https://arxiv.org/abs/1012.3224.

L. Hernquist. An analytical model for spherical galaxies and bulges. *The Astrophysical Journal*, 356:359–364, 1990. doi: 10.1086/168845.

Rodrigo A. Ibata, Khyati Malhan, and Nicolas F. Martin. The streams of the gaping abyss: A population of entangled stellar streams surrounding the inner galaxy. *The Astrophysical Journal*, 872(2):152, February 2019. ISSN 1538-4357. doi: 10.3847/1538-4357/ab0080. URL http://dx.doi.org/10.3847/1538-4357/ab0080.

Raul Jimenez. Globular clusterages. *Proceedings of the National Academy of Sciences*, 95(1):13–17, 1998. doi: 10.1073/pnas.95.1.13. URL https://www.pnas.org/doi/abs/10.1073/pnas.95.1.13.

E. M. Kirby, P. Guhathakurta, J. D. Simon, M. Geha, N. F. Martin, and M. Chou. The universal stellar mass–stellar metallicity relation for dwarf galaxies. *The Astrophysical Journal*, 779(2):102, 2013. doi: 10.1088/0004-637X/779/2/102.

Helmer H. Koppelman, Amina Helmi, Davide Massari, Sebastian Roelenga, and Ulrich Bastian. Characterization and history of the helmi streams with gaia dr2. *Astronomy Astrophysics*, 2018.

V. Kravtsov, G. Alcaíno, G. Marconi, and F. Alvarado. Evidence of the inhomogeneity of the stellar population in the differentially reddened globular cluster ngc 3201. *Astronomy and Astrophysics*, 512:L6, March 2010. ISSN 1432-0746. doi: 10.1051/0004-6361/200913749. URL http://dx.doi.org/10.1051/0004-6361/200913749.

Chengze Liu, Eric W. Peng, Elisa Toloba, J. Christopher Mihos, Laura Ferrarese, Karla Alamo-Martínez, Hong-Xin Zhang, Patrick Côté, Jean-Charles Cuillandre, Emily C. Cunningham, Puragra Guhathakurta, Stephen Gwyn, Gregory Herczeg, Sungsoon Lim, Thomas H. Puzia, Joel Roediger, Rubén Sánchez-Janssen, and Jun Yin. The most massive ultra-compact dwarf galaxy in the virgo cluster. *The Astrophysical Journal*, 812(1):L2, October 2015. ISSN 2041-8213. doi: 10.1088/2041-8205/812/1/l2. URL http://dx.doi.org/10.1088/2041-8205/812/1/L2.

Steven R. Majewski, M. F. Skrutskie, Martin D. Weinberg, and James C. Ostheimer. A 2mass all-sky view of the Sagittarius dwarf galaxy: I. Morphology of the Sagittarius core and tidal arms. *Astrophys. J.*, 599:1082–1115, 2003. doi: 10.1086/379504.

David Martínez-Delgado, Antonio Aparicio, M. Ángeles Gómez-Flechoso, and Ricardo Carrera. Tidal Streams in the Galactic Halo: Evidence for the Sagittarius Northern Stream or Traces of a New Nearby Dwarf Galaxy. , 549(2):L199–L202, March 2001. doi: 10.1086/319167.

D. Massari, H. H. Koppelman, and A. Helmi. Origin of the system of globular clusters in the milky way. *Astronomy Astrophysics*, 2019. doi: 10.1051/0004-6361/201936135.

Paul J. McMillan. The mass distribution and gravitational potential of the milky way. *Monthly Notices of the Royal Astronomical Society*, 465(1):76–94, October 2017. ISSN 1365-2966. doi: 10.1093/mnras/stw2759. URL http://dx.doi.org/10.1093/mnras/stw2759.

M. Miyamoto and R. Nagai. Three-dimensional models for the distribution of mass in galaxies. *Publications of the Astronomical Society of Japan*, 27:533–543, 1975.

European Southern Observatory. Ngc 3201: A beautiful globular cluster, 2021. URL https://www.eso.org/public/images/ngc3201/. Accessed: 2025-01-20.

OpenAI. Chatgpt (version 4). Online, 2024. Purpose: Gneral information for the Introduction and Methods sections. Used from December 2023 to February 2024. Available at https://openai.com/chatgpt.

H. C. Plummer. On the problem of distribution in globular star clusters. *Monthly Notices of the Royal Astronomical Society*, 71:460–470, 1911. doi: 10.1093/mnras/71.5.460.

Adrian Price-Whelan, Ana Bonaca, David W. Hogg, and Charlie Conroy. The GD-1 stellar stream suggests the existence of dark substructure in the Milky Way halo. 233: 129.08, January 2019.

Devesh P. Sariya, Ing-Guey Jiang, and R. K. S. Yadav. A Proper Motions Study of the Globular Cluster NGC 3201. , 153(3):134, March 2017. doi: 10.3847/1538-3881/aa5be6.

Linda S. Sparke and John S. III Gallagher. *Galaxies in the Universe: An Introduction*. Cambridge University Press, 2nd edition, 2007. ISBN 978-0521671866.

E. Tolstoy, V. Hill, M. Tosi, F. Primas, M. J. Irwin, M. D. Shetrone, T. A. Smecker-Hane, B. Letarte, P. Jablonka, M. Chiba, A. Koch, O. Y. Gnedin, and H. Ritcher. Star formation histories, abundances and kinematics of dwarf galaxies in the local group. *The Astrophysical Journal*, 690(2):267, 2009. doi: 10.1088/0004-637X/690/2/267.

Jacques P. Vallée. Meta-analysis from different tracers of the small local arm around the sun—extent, shape, pitch, origin. *Astrophysics and Space Science*, 363(11), October 2018. ISSN 1572-946X. doi: 10.1007/s10509-018-3463-2. URL http://dx.doi.org/10.1007/s10509-018-3463-2.

Eugene Vasiliev. Agama: action-based galaxy modelling architecture. *Monthly Notices of the Royal Astronomical Society*, 482(2):1525–1544, January 2019. doi: 10.1093/mnras/sty2672.

Laura L. Watkins, Roeland P. van der Marel, Sangmo Tony Sohn, and N. Wyn Evans. Evidence for an intermediate-mass milky way from gaia dr2 halo globular cluster motions. *The Astrophysical Journal*, 873(2):118, 2019. doi: 10.3847/1538-4357/ab089f.

N. A. Webb, P. J. Wheatley, and D. Barret. Xmm-newton x-ray and optical observations of the globular clusters m 55 and ngc 3201. *Astronomy amp; Astrophysics*, 445(1): 155–165, December 2005. ISSN 1432-0746. doi: 10.1051/0004-6361:20053010. URL http://dx.doi.org/10.1051/0004-6361:20053010.